



1 **A biophysical approach using drought stress factor for daily estimations of**
2 **evapotranspiration and CO₂ uptake in high-energy water-limited**
3 **environments**

4

5

6

7 David Helman^{1,2,*}, Itamar M Lensky¹, Yagil Osem³, Shani Rohatyn⁴, Eyal Rotenberg⁴ and Dan
8 Yakir⁴

9

10

11 ¹ Department of Geography and Environment, Bar Ilan University, Ramat Gan 52900, Israel

12 ² Department of Geography, University of Cambridge, Cambridge, CB2 3EN, UK

13 ³ Department of Natural Resources, Agricultural Research Organization, Volcani Center, Bet
14 Dagan 50250, Israel

15 ⁴ Earth and Planetary Sciences, Weizmann Institute of Science, Rehovot 76100, Israel

16

17

18

19 *Corresponding author:

20 David Helman (dh565@cam.ac.uk ; davidhelman.biu@gmail.com)

21 Department of Geography, Bar-Ilan University, Ramat Gan 52900

22 Israel.

23 Tel: +972 3 5318342

24 Fax: +972 3 5344430

25 **Abstract**

26

27 Estimations of ecosystem-level evapotranspiration (ET) and CO₂ uptake in water-limited
28 environments are scarce and scaling up ground-level measurements is not straightforward. A
29 biophysical approach was previously proposed for ecosystem-level assessment relying on
30 vegetation index and meteorological data (RS-Met) in temperate Mediterranean ecosystems.
31 However, these RS-Met models have not been tested yet in extreme high-energy water-
32 limited ecosystems that suffer from continuous stress conditions. Owing to the lack of ET and
33 CO₂ flux estimations in the Eastern Mediterranean, we examined the RS-Met approach using
34 a newly developed mobile lab system and the single active Fluxnet station operating in this
35 region, in seven forest and non-forest sites across a climatic transect in Israel (280-770 mm y⁻¹).
36 The RS-Met models were used with and without the addition of a seasonal drought stress
37 factor (f_{DS}), which was based on daily rainfall, temperature and radiation data.

38 Results show that the RS-Met models with the inclusion of the f_{DS} were significantly
39 improved compared to the non- f_{DS} models ($r=0.64-0.91$ compared to $0.05-0.80$; $P=0.06$ and
40 $r=0.72-0.92$ compared to $r=0.56-0.90$; $P<0.01$ for ET and GPP, respectively). These,
41 successfully tracked observed seasonal changes in ET and GPP across sites ($ET_{MOD} =$
42 $0.94 \times ET_{EC} + 0.28$; $r=0.82$; $MAE=0.54$ mm d⁻¹; $N=243$ d, and $GPP_{MOD} = 0.99 \times GPP_{EC} +$
43 0.51 ; $r=0.86$; $MAE=1.03$ gC m⁻² d⁻¹; $N=252$ d). Modeled ET and GPP also agreed well with
44 eddy covariance estimates at the annual timescale in the Fluxnet station located in the dryland
45 pine forest of Yatir (266 ± 61 vs. 257 ± 58 mm y⁻¹ and 765 ± 112 vs. 748 ± 124 gC m⁻² y⁻¹ for ET
46 and GPP, respectively). Using the RS-Met models, we were able to show the effect of
47 afforestation on water vapor and CO₂ fluxes in this region. Afforestation was responsible for
48 a significant increase in water use efficiency (WUE) with positive effect decreasing when
49 moving from dry to more humid environments, strengthening the importance of drylands
50 afforestation. This simple but yet robust biophysical approach show a promise for reliable
51 ecosystem-level estimations of ET and CO₂ uptake in extreme high-energy water-limited
52 environments when adjusting for drought stress effects.

53

54 **Keywords:** CO₂; drought stress; ET; GPP; MODIS; NDVI



55 1. Introduction

56 Assessing the water use and carbon uptake in terrestrial ecosystems is of the utmost
57 importance for monitoring biosphere responses to climate change (Ciais et al., 2005; Jung et
58 al., 2010; Reichstein et al., 2013). Accurate estimations of evapotranspiration (ET) and gross
59 primary production (GPP), as a measure of the CO₂ uptake, usually require the integration of
60 extensive meteorological, flux and field-based data (e.g., Wang *et al.*, 2014; Kool *et al.*,
61 2014). Measurements of leaf gas exchange and isotopic composition (e.g., $\delta^{13}\text{C}$ and $\delta^{18}\text{O}$)
62 have been used to estimate leaf-scale carbon and water fluxes (Klein et al., 2013; Maseyk et
63 al., 2011; Raz-Yaseef et al., 2012a). Meanwhile, observations of sap flow and tree rings often
64 serve to estimate fluxes at the tree-level (Klein et al., 2016; Wang et al., 2014). However,
65 scaling up such measurements to the ecosystem level is not straightforward and require the
66 use of complex models (Way et al., 2015).

67

68 Currently, the eddy covariance (EC) technique is the most direct method for measuring
69 carbon and water vapor fluxes at the ecosystem level (Baldocchi, 2003). The EC approach
70 benefits from continuous temporal coverage; currently (April, 2017), there are more than 560
71 active EC sites across the globe, as part of the Fluxnet program (<http://fluxnet.ornl.gov>).
72 However, there are also some practical and technical limitations. The EC measurement is
73 representative of a relatively small area (<2 km²), and the application of the EC approach is
74 limited to relatively homogeneous and flat terrains. Additionally, most EC towers are
75 concentrated in the US, Europe and Asia, with poor coverage in water-limited regions, such
76 as North Africa and the Eastern Mediterranean (Schimel et al., 2015).

77

78 Remote-sensing-based models (RS models) have been used to overcome some of the
79 limitations of EC, complementing the information derived from the flux towers. In contrast to
80 process-driven models, RS models benefit from continuous, direct observation of the Earth's
81 surface, acquiring data at a relatively high spatial resolution and with full regional to global
82 coverage. Many RS models for the estimation of ET and GPP exist (see review in Kalma *et*
83 *al.*, 2008), but most of them are too complex, with low accessibility for researchers outside
84 the remote sensing community.

85

86 In the past decade, several simple biophysical ET and GPP models based on vegetation
87 indices (from satellite data) have emerged, offering assessment at relatively high to moderate



88 spatial and temporal resolutions and with acceptable accuracy (Veroustraete *et al.*, 2002;
89 Sims *et al.*, 2008; Maselli *et al.*, 2009, 2014; and see also the review in Glenn *et al.*, 2010).
90 One of those models is the ET model based on the FAO-56 formulation (Allen *et al.*, 1998).
91 This model uses a function of satellite-derived vegetation index, usually the normalized
92 difference vegetation index (NDVI), as a substitute for the crop coefficient, which is defined
93 as the ratio of the actual to the potential ET (ET_0) in the FAO-56 formulation. Being a
94 measure of the green plant biomass and the ecosystem leaf area, the NDVI is often used as a
95 surrogate for plant transpiration and rainfall interception capacity (Glenn *et al.*, 2010).
96 Additionally, the NDVI is closely related to the radiation absorbed by the plant and to its
97 photosynthetic capacity (Gamon *et al.*, 1995). However, the direct detection, through NDVI,
98 of the abovementioned parameters at a seasonal timescale is still challenging and usually
99 requires additional meteorological information (Helman *et al.*, 2015a). The RS model based
100 on the FAO-56 formulation combines the two sources of information, satellite and
101 meteorological, providing a daily estimation of actual ET. This model, originally proposed
102 for croplands and other managed vegetation systems (Allen *et al.*, 1998; Glenn *et al.*, 2010),
103 was recently adjusted for applications in natural vegetation systems by Maselli *et al.* (2014).

104

105 For the estimation of GPP, a simple but robust biophysical GPP model is the one based on
106 the radiation use efficiency (RUE) model proposed by Monteith (1977). The classical
107 Monteith-type model depends on the absorbed radiation and on the efficiency of the
108 vegetation at converting this radiation into carbon-based compounds. Accordingly, this
109 Monteith-based model is driven by radiation and temperature data, acquired from
110 meteorological stations, and by the fraction of photosynthetically active radiation ($fPAR$),
111 which can be calculated from the satellite-derived NDVI or EVI. A major challenge in this
112 model, however, is the estimation of the RUE, a key component of the model, which usually
113 depends on plant species type and environmental conditions. Currently, the conventional
114 procedure is to use a plant-species-dependent maximum RUE from a lookup table and adjust
115 it for seasonal changes using some sort of a factor that changes throughout the season based
116 on meteorological data (Running *et al.*, 2004; Zhao and Running, 2010).

117

118 Though simple, both ET and GPP models (hereafter RS-Met models) were shown to be
119 promising in accurately assessing daily ET and GPP at a relatively high spatial resolution (<1
120 km) (Helman *et al.*, 2017; Maselli *et al.*, 2014, 2006; Veroustraete *et al.*, 2002). However, the
121 use of the RS-Met models is limited to ecosystems under normally non-stressful conditions



122 because there is no accurate representation of water availability in these models. Recently,
123 the incorporation of a drought-stress factor (f_{DS}) in these models was proposed by Maselli *et*
124 *al.*, (2009, 2014), adjusting for short-term stress conditions in water-limited natural
125 ecosystems. The proposed f_{DS} is based only on daily rainfall data and daily potential ET
126 calculated from temperature and/or incoming radiation. The RS-Met models with the addition
127 of the f_{DS} were successfully validated against EC-derived estimates of ET and GPP in several
128 sites in Italy (Maselli *et al.*, 2014, 2009, 2006).

129

130 However, the RS-Met approach has never been tested in extreme high-energy water-limited
131 environments such as those in the Eastern Mediterranean. Currently, there is only one active
132 Fluxnet station in the entire Eastern Mediterranean (Yatir forest, southern Israel; Fig. 1a) that
133 measures water vapor and carbon fluxes (since 2000); while in this region water is considered
134 to be a valuable resource and the proper management of this resource depends on the accurate
135 assessment of the ET component. Moreover, despite of the well-known important
136 contribution of this region to the global CO₂ (Ahlström *et al.*, 2015), there are almost no
137 efforts of estimating CO₂ fluxes in forested and non-forested areas in this region. This led to
138 the development of the Weizmann mobile lab system (Israel; Fig. 1h) that allows extension of
139 the permanent Fluxnet measurement sites on campaign basis (e.g., Asaf *et al.*, 2013; for
140 technical detail see: <http://www.weizmann.ac.il/EPS/Yakir/node/321>). Such a system could
141 allow flux and auxiliary analytical measurements across a range of climatic conditions, plant
142 species and ecosystems, as well as addressing land use changes and disturbance. However, to
143 extend these campaign-based measurements in time and space a model fitted to the high-
144 energy water-limited conditions of this region is required.

145

146 Here, we tested the RS-Met approach in a total of seven ecosystems distributed at three
147 precipitation levels along a rainfall gradient (280-770 mm y⁻¹) in the Eastern Mediterranean
148 region (Israel; Fig. 1). Ecosystems included three pairs of planted forests and adjacent non-
149 forest sites (representing the original area on which these forests were planted). Ground-level
150 campaign measurements of ET and net ecosystem CO₂ exchange using the newly developed
151 mobile lab (Fig. 1h) and the continuous flux measurements in the active Fluxnet site in Yatir
152 (Klein *et al.*, 2016; Tatarinov *et al.*, 2016) were used to validate the RS-Met models. This
153 combination of model-based estimates and direct flux measurements of ET and CO₂ uptake
154 across a range of climatic conditions and ecosystems provides a unique opportunity to test
155 and validate the RS-Met approach in this high-energy water-limited region. Particularly, we



156 examined the RS-Met models with and without the application of the f_{DS} , which was
157 originally proposed by Maselli *et al.* (2014) for temperate Mediterranean environments.
158 Thus, our specific goals in this study were: (1) examine the seasonal evolution of f_{DS} and its
159 role in the estimation of the fluxes from the RS-Met models in these environments, (2)
160 compare the model estimates with EC measurements across these high-energy water-limited
161 sites, at a daily and annual scale, with and without the use of the f_{DS} , and (3) use the best RS-
162 Met models to estimate changes in water use efficiency ($WUE=GPP/ET$) following
163 afforestation across the rainfall gradient in Israel, by comparing the three-paired forest vs.
164 non-forest sites.

165

166

167 2. Materials and methods

168 2.1. Study sites

169 The sites in this study included three pairs of planted pine forests (*Pinus halepensis* Mill.)
170 and adjacent non-forested (dwarf shrublands) sites distributed throughout a climatic range in
171 Israel ($P = 280 - 770 \text{ mm y}^{-1}$), from dry to sub-humid Mediterranean (Table 1 and Fig. 1a-f),
172 which represent the typical Mediterranean vegetation systems in the Eastern Mediterranean.
173 The three non-forested sites represent the original natural environment on which the pine
174 forests were planted, while the afforested sites are currently managed by the Jewish National
175 Fund (KKL). The non-forested shrubland sites are mostly dominated by *Sarcopoterium*
176 *spinosum* (dwarf shrub) in a patchy distribution with a wide variety of herbaceous species,
177 mostly annuals, growing in between the shrub patches during winter to early spring. In
178 addition, we tested the models in one native deciduous forest site dominated by *Quercus*
179 species. A brief description of the sites is given in the following:

180

181 *Yatir*. The forest of Yatir is an Aleppo pine forest (*Pinus halepensis*) that was planted by
182 KKL mostly during 1964-1969 in the semiarid region of Israel (31.34N, 35.05E; Fig. 1a). It
183 covers a total area of *c.* 2800 ha and lies on a predominantly light brown Rendzinas soil ($79 \pm$
184 45.7 cm deep), overlying a chalk and limestone bedrock (Llusia *et al.*, 2016). The average
185 elevation is 650 m. The mean annual rainfall in the forest area is 285 mm y^{-1} (for the last 40
186 years) and was 279 mm y^{-1} in the Fluxnet site during 2001-2015 (Table 1). The mean annual
187 temperature in Yatir is $18.2 \text{ }^\circ\text{C}$ with 13 and $31 \text{ }^\circ\text{C}$ for mean winter (November– January) and
188 summer (May–July) temperatures, respectively. Tree density in Yatir is *c.* $300 \text{ trees ha}^{-1}$



189 (Rotenberg and Yakir, 2011) with a tree average height of *c.* 10 m and canopy leaf area index
190 (LAI) of $1.4 \pm 0.4 \text{ m}^2 \text{ m}^{-2}$, which displays small fluctuations between winter and summer
191 (Sprintsin et al., 2011). The understory in this forest is mostly comprised of ephemeral
192 herbaceous species (*i.e.*, therophytes, geophytes and hemicryptophytes) growing during the
193 wet season (September-April) and drying out in the beginning of the dry season (May-June).
194 A relatively thin needle litter layer covers the forest floor during the needle senescence period
195 (June-August) (Maseyk et al., 2008).

196
197 *Eshtaol*. The forest of Eshtaol was planted in the late 1950's by KKL with mostly *P.*
198 *halepensis* trees in the central part of Israel (31.79N, 34.99E; Fig. 1c). The current forest area
199 is *c.* 1200 ha and lies mainly on Rendzinas soils. The average elevation is 330 m. The mean
200 annual rainfall in this area is *c.* 500 mm y^{-1} and was a 480 mm y^{-1} in the site of the EC
201 measurements during 2012-2015 (Table 1). Tree density in Eshtaol is typically 300–350 trees
202 ha^{-1} , with a tree canopy LAI that ranges between $1.9 \text{ m}^2 \text{ m}^{-2}$ and $2.6 \text{ m}^2 \text{ m}^{-2}$ and a tree average
203 height of 12.5 m (Osem et al., 2012).

204
205 *Birya*. The forest of Birya is a *P. halepensis* forest that was mostly planted during the early
206 1950's in the northern part of Israel, Galilee region (33.00N, 35.48E; Fig. 1e). The forest
207 covers an area of *c.* 2100 ha and lies on a Rendzinas and Terra rossa soils. The average
208 elevation is 730 m. The average temperature in this area is 16°C, with an average annual
209 rainfall of 710 mm y^{-1} and 776 mm y^{-1} during the years of the EC measurements (2012-2015;
210 Table 1). The average stand density is 375 trees ha^{-1} with an average tree height of 11 m
211 (Llusia et al., 2016).

212
213 *HaSolelim*. The HaSolelim forest is a native deciduous mixed oak forest dominated by
214 *Quercus ithaburensis*, which is accompanied by *Quercus calliprinos* (evergreen) and few
215 other Mediterranean broadleaved tree and shrub species (Fig. 1g). The forest is located at the
216 northern part of Israel in the Galilee region, 30 km south of the Birya forest (32.74N,
217 35.23E). The forest covers an area of *c.* 240 ha and lies on Rendzinas and Terra rossa soils.
218 The elevation in the site of the EC measurements is 180 m (Table 1). The average
219 temperature in this area is a typically 21°C, with a mean annual rainfall of 580 mm y^{-1} and
220 543 mm during the years of the EC measurements. The site where the measurements took
221 place is characterized by an average stand density of 280 trees ha^{-1} and an average tree height
222 of 8 m (Llusia et al., 2016).



223

224 *Wady Attir*. This is a xeric shrubland site located southwest to the forest of Yatir (31.33N,
225 34.99E). The average elevation is 490 m. The site is dominated by semi-shrubs species such
226 as, *Phagnalon rupestre* L, with *graminae* species, mainly *Stipa capensis* L. (also known as
227 Mediterranean needle grass), *Hordeum spontaneum* K. Koc. (also known as wild barley) and
228 some *Avena* species such as, *A. barbata* L. and *A. sterilis* L., appearing shortly after the rainy
229 season (Leu et al. 2014; Fig. 1b). The mean annual rainfall in this area is 230 mm y^{-1}
230 (Mussery et al., 2016) and was 280 mm y^{-1} in the years of the EC measurements (2012-2015;
231 Table 1).

232

233 *Modiin*. The shrubland site of Modiin is located few kilometers from the forest site of Eshtaol
234 and represent the original environment on which this forest was planted (31.87N, 35.01E;
235 Fig. 1d). The average elevation is 245 m. The shrubland site is mostly dominated by
236 *Sarcopoterium spinosum* (dwarf shrub) in a patchy distribution with a wide variety of
237 herbaceous species, mostly annuals, growing in between the shrub patches during winter to
238 early spring. The average rainfall amount in this area was 480 mm y^{-1} in the years of the EC
239 measurements (Table 1).

240

241 *Kadita*. The shrubland site of Kadita is also dominated by *Sarcopoterium spinosum* (dwarf
242 shrub) in a typical patchy distribution (Fig. 1f). It is located nearby the forest of Birya at an
243 elevation of 815 m (33.01N, 35.46E; Table 1). The mean annual rainfall in this site is similar
244 to that recorded in the Birya forest (i.e., 766 mm y^{-1} in the years of study).

245

246 All shrubland sites have been under continuous livestock grazing for many years, and their
247 vegetation structures are mainly the outcome of both rainfall amount and grazing regime.

248

249 2.2. Satellite-derived vegetation index

250 We used the NDVI from the moderate-resolution imaging spectroradiometer (MODIS) on
251 board NASA's Terra satellite at 250 m spatial resolution (MOD13Q1). The MOD13Q1
252 NDVI product is a composite of a single day's value selected from 16-day periods based on
253 the maximum value criteria (Huete et al., 2002). The Terra's NDVI product is acquired
254 during the morning (10:30 am) and thus provides a good representation of the peak time of
255 the plants' diurnal activity. The gradual growth of the vegetation enables the interpolation of



256 the 16-day NDVI time series to representative daily values (Glenn et al., 2008; Maselli et al.,
257 2014). We downloaded the 16-day NDVI time series covering the main area of the eddy
258 covariance flux measurement for each site from the MODIS Subsets
259 ([http://daacmodis.ornl.gov/cgi-](http://daacmodis.ornl.gov/cgi-bin/MODIS/GLBVIZ_1_Glb/modis_subset_order_global_col5.pl)
260 [bin/MODIS/GLBVIZ_1_Glb/modis_subset_order_global_col5.pl](http://daacmodis.ornl.gov/cgi-bin/MODIS/GLBVIZ_1_Glb/modis_subset_order_global_col5.pl)) for the period October
261 2001 – October 2015. Then, we pre-processed the NDVI time series as described in Helman
262 et al. (2014a, 2014b, 2015b) to remove outliers and uncertainties due to cloud contamination
263 and atmospheric disturbances. The processed 16-day NDVI time series were then
264 interpolated on a daily basis using the local scatterplot smoothing technique (LOESS). This
265 technique is suited for eliminating outliers in non-parametric time series and has been shown
266 to be a useful tool in the interpolation of datasets with a seasonal component (Cleveland,
267 1979).

268

269 2.3. The mobile lab system and the Fluxnet station in Yatir

270 A newly designed mobile flux measurement system was used in all campaigns (Fig. 1h),
271 based on the 28-m pneumatic mast on a 12-ton 4x4 truck that included a laboratory providing
272 an air-conditioned instrument facility (cellular communication, 18 KVA generator, 4200
273 WUPS). Flux, meteorological and radiation measurements relied on an eddy-covariance
274 system that provides CO₂ measurements and sensible and latent heat fluxes using a three-
275 dimensional sonic anemometer (R3, Gill Instruments, Lymington, Hampshire, UK) and
276 enclosed-path CO₂-H₂O IRGA (Licor 7200, Li-Cor, Lincoln, NE, USA) using
277 CarboEuroFlux methodology (Aubinet et al., 2000), and EddyPro Software (www.licor.com).
278 Data were collected using self-designed program in LabVIEW software. Air temperature and
279 relative humidity (HMP45C probes, Campbell Scientific) and air pressure (Campbell
280 Scientific sensors) were measured at 3 m above the canopy. Energy fluxes relied on radiation
281 sensors, including solar radiation (CMP21, Kipp and Zonen), long-wave radiation (CRG4,
282 Kipp and Zonen) and photosynthetic radiation (PAR, PAR-LITE2) sensors. All sensors were
283 installed in pairs facing both up and down and are connected using the differential mode
284 through a multiplexer to a data logger (Campbell Scientific). GPP for each site was estimated
285 from the measured net ecosystem CO₂ exchange (NEE) using the conventional approach of
286 estimating ecosystem respiration, Re, and a regression of NEE on turbulent nights against
287 temperature, followed by extrapolating the derived night-time Re-temperature relationship to
288 daytime periods (Reichstein *et al.*, 2005; modified for our region by Afik, 2009). Flux



289 measurements with the mobile system were carried out on a campaign basis, in six of the
290 seven sites, with each campaign representing approximately two weeks in a single site,
291 repeated along the seasonal cycle with mostly two but sometimes only one two-weeks set of
292 measurements per cycle, during the 4 years of measurements, 2012-2015. Continuous flux
293 measurements were carried out in the permanent Fluxnet site of Yatir (xeric forest site).
294 Begun in 2000, the eddy covariance (EC) and supplementary meteorological measurements
295 have been conducted continuously (Rotenberg and Yakir, 2011; Tatarinov et al., 2016), with
296 measurements performed according to the Euroflux methodology. Instrumentation is similar
297 to that in the Mobile Lab except for the use of a closed-path CO₂/H₂O infrared gas analyzer
298 (IRGA, LI- 7000; Li-Cor, Lincoln, NE) with the inlet placed 18.7 m above ground. Typical
299 fetch providing 70% (cumulative) contribution to turbulent fluxes was measured between 100
300 m and 250 m (depending on the site) along the wind distance. This was taken in consideration
301 when using the MOD13Q1 product to derive the modeled fluxes.

302

303 Daily estimates of potential evapotranspiration, i.e. ET_o (in mm d⁻¹), for the ET model, the
304 drought stress factor and the water availability factor, were calculated from the mean daily air
305 temperature and the daily total incoming solar radiation, measured at the seven sites
306 following the empirical formulation proposed by Jensen & Haise (1963):

307

$$308 \quad ET_o = \frac{R_g}{2470} (0.078 + 0.0252 T) \quad (1)$$

309

310 where T is the mean daily air temperature (in °C), and R_g is the daily global (total) incoming
311 solar radiation (in kJ m⁻² d⁻¹); ET_o is finally converted into mm d⁻¹ by dividing the R_g by 2470
312 mm kJ m⁻² d⁻¹ (see in Jensen & Haise, 1963). We decided to use this ET_o formulation of
313 Jensen & Haise (1963) to be consistent with the original RS-Met proposed by Maselli et al.
314 (2014) though we are aware of the large tradition of works devoted to compare several
315 methods to estimate ET_o, and to prove the validity and limitations of these methods under
316 different environmental conditions.

317

318 2.4. The PaVI-E model for annual ET

319 We used the PaVI-E model (Parameterization of Vegetation Index for the estimation of ET;
320 Helman et al., 2015a) to validate the ET from the RS-Met model on an annual basis, owing to



321 the lack of continuous flux measurements in six of the seven sites (Eshtaol, HaSolelim, Biryā,
322 Wady Attir, Modiin and Kadita, see Table 2 for N of the EC flux measurements in each of
323 those sites). The PaVI-E is an empirical model based on the simple relationships between
324 MODIS-derived EVI and NDVI and annual ET measured with EC in 16 Fluxnet sites,
325 comprising a wide range of plant functional types across Mediterranean-climate regions. The
326 PaVI-E model produces annual ET at a spatial resolution of 250 m and was validated against
327 physical-based models (MOD16 and MSG LSA-SAF ETa) and ET retrieved from water
328 balances across the same study area (Helman et al., 2015a). It was shown to be useful for
329 ecohydrological study in this region, providing insights into the role of climate in altering
330 forest water and carbon cycles (Helman et al., 2017, 2016). The advantage of PaVI-E is that
331 it does not require any additional meteorological information but is a function of the satellite-
332 derived vegetation indices alone. This makes it interesting to compare with the RS-Met
333 model since the RS-Met is highly dependent on meteorological forcing.

334

335

336 3. Description of the models and the use of a drought stress factor

337 The RS-Met models used here for the daily estimation of ET and GPP are based on the NDVI
338 and the meteorological data (Maselli et al., 2014, 2009, 2006; Veroustraete et al., 2002). Each
339 model was applied with (DS) and without (no-DS) a drought stress adjustment (i.e., two
340 models for ET and two for the GPP).

341

342 3.1. The ET model

343 The RS-Met model of daily ET is based on the FAO-56 formulation (Eq. 2):

344

$$345 \text{ET} = \text{ET}_0 \times (K_C + K_S) \quad (2)$$

346

347 Where K_C and K_S stand for the crop/canopy and soil coefficients, respectively (Allen et al.,
348 1998). In the RS-Met model a maximum value of K_C (K_{C_max}), which depends on the type of
349 the monitored vegetation (Allen et al., 1998; Maselli et al., 2014), and a maximum value of
350 K_S (K_{S_max}), for soil evaporation, are used as a reference in the model. The K_{C_max} and K_{S_max}
351 are then multiplied by a linear transformation of the NDVI (i.e., $f(\text{NDVI})$ and $f(1-\text{NDVI})$,
352 respectively) to adjust for the seasonal evolution of the crop/canopy and soil coefficients:



353

$$354 \quad K_C = K_{C_max} \times f(\text{NDVI}) \quad (3)$$

355

$$356 \quad K_S = K_{S_max} \times f(1-\text{NDVI}) \quad (4)$$

357

358 Following Maselli *et al.* (2014), we used here the fractional vegetation cover (fVC) to better
 359 represent both ET processes: direct soil evaporation and plant transpiration. The fVC is a
 360 classical two-end member function based on minimum and maximum values of NDVI,
 361 corresponding to a typical soil background without vegetation ($\text{NDVI}_{\text{SOIL}}$) and an area fully
 362 covered by vegetation (NDVI_{VEG}), respectively:

363

$$364 \quad fVC = (\text{NDVI} - \text{NDVI}_{\text{SOIL}}) / (\text{NDVI}_{\text{VEG}} - \text{NDVI}_{\text{SOIL}}) \quad (5)$$

365

366 Thus, Eqs. (3) and (4) become:

367

$$368 \quad K_C = K_{C_max} \times fVC \quad (6)$$

369

370 and

371

$$372 \quad K_S = K_{S_max} \times (1-fVC), \quad (7)$$

373

374 respectively.

375

376 The fVC in Eq. (5) is calculated on a daily basis from the interpolated NDVI (daily) data.
 377 Note that the fVC in Eq. (6) represents the fraction of the area covered by the vegetation,
 378 while in Eq. (7) the term $1-fVC$ represents the fraction of the bare soil area. Both terms, fVC
 379 and $1-fVC$ in Eqs. (6) and (7), change over the course of a year due to canopy development
 380 and/or the appearance of ephemeral herbaceous plants. We used here the values of 0.1 and
 381 0.8 for the $\text{NDVI}_{\text{SOIL}}$ and NDVI_{VEG} , respectively, as proposed in Helman *et al.*, (2015b) for
 382 this region.

383

384 Finally, from Eqs. (2) and (5-7) we obtain the model without the drought stress adjustment
 385 (no-DS):



386

$$ET = ET_o \times \{fVC \times K_{C_max} + [(1-fVC) \times K_{S_max}]\} \quad (8)$$

388

389 Following Maselli *et al.* (2014), we used the drought stress factor (f_{DS}) and the water
 390 availability factor (f_{WA}) to adjust the crop/canopy and soil coefficients for stressful conditions
 391 in Eqs. (6) and (7), respectively:

392

$$K_C = K_{C_max} \times fVC \times f_{DS} \quad (9)$$

394

395 and

396

$$K_S = K_{S_max} \times (1-fVC) \times f_{WA} \quad (10)$$

398

399 The f_{DS} and f_{WA} in Eqs. (9) and (10) simulate the effects of drought stress and available water
 400 (or water shortage) for plant transpiration and bare soil evaporation, whereas the f_{DS} is
 401 defined as follows (Maselli *et al.*, 2014):

402

$$f_{DS} = 0.5 + 0.5 \times f_{WA} \quad (11)$$

404

405 The water availability factor (f_{WA}) is calculated as the simple ratio between the daily rainfall
 406 amount and the daily ET_o , both cumulated over a period of two months (Maselli *et al.*, 2014).
 407 The f_{WA} is set to 1 when the cumulated rainfall amount exceeds the atmospheric demand (i.e.,
 408 the ET_o). Note that the f_{DS} would then vary between 0.5 and 1, meaning that ET is reduced to
 409 half the potential maximum in the absence of water supply, simulating the basic transpiration
 410 levels maintained by evergreen vegetation (Glenn *et al.*, 2011 and see also in Maselli *et al.*
 411 2014). This reduction in the f_{DS} accounts for the short-term stress effects on plant
 412 transpiration, while long-term effects that cause damage to the function of the plant would be
 413 mainly reflected through changes in the NDVI/ fVC (Glenn *et al.*, 2010; Running and Nemani,
 414 1988). In contrast to the f_{DS} , the f_{WA} is reduced to zero following a dry period longer than two
 415 months, making the surface evaporation component null during the dry summer. Basically,
 416 the accumulation period could vary for different ecosystem types. However, we have taken
 417 here a period of two months for the native shrublands and planted (and native) forests



418 following Maselli et al. (2014) that suggested the use of a longer period (two months) for
419 such ecosystems compared to the short period (one month) often used for annual crops.

420

421 Replacing Eqs. (6) and (7) by Eqs. (9) and (10) the no-DS model (Eq. 8) becomes the
422 following DS model:

423

$$424 \quad ET = ET_0 \times \{fVC \times K_{C_max} \times f_{DS}\} + \{(1-fVC) \times K_{S_max} \times f_{WA}\} \quad (12)$$

425

426 Here we used a K_{C_max} value of 0.7 for both forests and non-forest sites, and a K_{S_max} value of
427 0.2 for soil evaporation in both DS and no-DS models, as previously proposed by Maselli et
428 al., (2014) for similar woody-dominated ecosystems.

429

430 Finally, both the DS (Eq. 12) and no-DS (Eq. 8) models derive daily ET estimates (in mm d⁻¹)
431 at the spatial resolution of the MODIS NDVI product, i.e., 250 m.

432

433 3.2. The GPP model

434 For the GPP model, we used the biophysical radiation use efficiency model proposed by
435 Monteith (1977):

436

$$437 \quad GPP = RUE \times fPAR \times PAR \quad (13)$$

438

439 where PAR is the daily incident photosynthetic active radiation (in MJ m⁻²), calculated as
440 45.7% from the incoming measured global solar radiation (Nagaraja Rao, 1984), and $fPAR$ is
441 the fraction of the PAR that is actually absorbed by the canopy (range from 0 to 1). The $fPAR$
442 was derived here from the daily NDVI time series following the linear formulation proposed
443 by Myneni & Williams (1994), which was successfully applied in similar remote-sensing-
444 based GPP models for similar ecosystems by Veroustraete *et al.* (2002) and Maselli *et al.*
445 (2006, 2009); RUE is the radiation use efficiency (in g C MJ⁻¹), which is the efficiency of the
446 plant for converting the absorbed radiation into carbon-based compounds and which changes
447 over the course of a year (Garbulska *et al.*, 2008).

448

449 The RUE is an important component in the GPP model and is the most challenging parameter
450 to compute. It is usually considered to be related to vapor pressure deficit, water availability,



451 temperature and plant species type (Running *et al.*, 2000), and there have been several recent
 452 efforts to directly relate it to the photochemical reflectance index (PRI), which can also be
 453 derived from satellites (Garbulsky *et al.*, 2014; Peñuelas *et al.*, 2011; Wu *et al.*, 2015).
 454 Currently, the conventional modeling of RUE for Mediterranean ecosystems is not
 455 straightforward and is mostly site specific, derived for specific local conditions (Garbulsky *et al.*,
 456 2008). Here, we used the simple approach proposed by Veroustraete *et al.*, (2002) and
 457 further developed by Maselli *et al.*, (2009), which states that a potential RUE (RUE_{MAX} in g
 458 C MJ⁻¹) can be adjusted for seasonal changes using a function based on temperature and
 459 water stress conditions (f_{WT}):

$$461 \quad \text{RUE} = \text{RUE}_{\text{MAX}} \times f_{\text{WT}} \quad (14)$$

462
 463 The f_{WT} adjusts the RUE_{MAX} for seasonal changes following changes in water availability and
 464 temperature conditions:

$$466 \quad f_{\text{WT}} = T_{\text{CORR}} \times f_{\text{DS}} \quad (15)$$

467
 468 where T_{CORR} is a temperature correction factor calculated on a daily basis (Veroustraete *et al.*,
 469 2002):

$$471 \quad T_{\text{CORR}} = \frac{e^{\left(\frac{a - \Delta H_{AP}}{G \cdot T}\right)}}{1 + e^{\left(\frac{\Delta S \cdot T - \Delta H_{DP}}{G \cdot T}\right)}} \quad (16)$$

472
 473 where a is a constant equal to 21.9; ΔH_{AP} and ΔH_{DP} are the activation and deactivation
 474 energies (in J mol⁻¹), equal to 52750 and 211, respectively; G is the gas constant, equal to
 475 8.31 J K⁻¹ mol⁻¹; ΔS is the entropy of the denaturation of CO₂ and is equal to 710 J K⁻¹ mol⁻¹;
 476 and T is the mean daily air temperature (in Kelvin degrees); and f_{DS} is the same drought-
 477 stress factor as in Eq. (11).

478
 479 The drought stress factor, f_{DS} , is used here only in the DS model (i.e., the model that
 480 considers drought stress conditions). Thus, in the no-DS model, the f_{WT} would be only a
 481 function of the temperature, and thus $f_{\text{WT}} = T_{\text{CORR}}$ (in Eq. 15). Following Garbulsky *et al.*,



482 (2008) and Maselli *et al.*, (2009), a constant value of 1.4 g C MJ^{-1} was used here for RUE_{MAX}
483 in all sites and models (i.e., the DS and no-DS).

484

485 Finally, daily GPP values were computed from both the DS and no-DS models, at a spatial
486 resolution of 250 m for each of the seven sites and compared with the EC measurements. It
487 should be stated that the use of the EC-derived GPP as a reference in the validation should be
488 taken with caution because GPP by itself is modeled and not directly measured. This may
489 introduce uncertainties to the validation that could be contaminated by self-correlation.

490

491

492 **4. Testing the drought stress factor in high-energy water-limited environments**

493 To show the importance of the drought stress factor (f_{DS}) in tracking the seasonal variation in
494 the fluxes at high-energy water-limited environments, we demonstrate the seasonal evolution
495 of f_{DS} together with the main components of the RS-Met models at one selective site (Fig. 2).
496 Figure 2a shows that the f_{DS} moderate the increase of K_C in the forest site of Eshtaol at the
497 beginning of the rainy season (October-December) even though the f_{VC} is relatively high due
498 to the appearance of ephemeral herbaceous vegetation in the understory (Helman *et al.*,
499 2015b). This is a realistic scheme since the herbaceous vegetation has little contribution to
500 the ecosystem fluxes but a significant contribution to the NDVI (and thus to the f_{VC}) signal
501 (Helman, n.d.). Thus, the f_{DS} has an important role in reducing the K_C to a more realistic low
502 value at this stage of the year when there is less water available for the trees (Fig. 2a). The
503 same applies for the end of the rainy season, in April-May, when both the ET_0 and the f_{VC}
504 are relatively high but there is almost no available water for ET, as implied from the low f_{DS}
505 (Fig. 2).

506

507 In the GPP model, the f_{DS} reduces the high RUE at both ends of the rainy season, adjusting
508 the GPP to the stress conditions during these periods (Fig. 2b). Particularly noted is the
509 significant reduction in GPP at the end of the rainy season (April-May), when both the PAR
510 and the RUE are high but less water is available for transpiration.

511

512

513 **5. Comparisons with the Fluxnet station in Yatir**

514 *5.1. Daily ET and GPP*



515 We compared the daily estimates of the modeled ET with the active Fluxnet station at the
516 dryland pine forest of Yatir (Table 1). As expected from the noted above (Section 4), the
517 model without the drought stress factor (no-DS) overestimated the ET in comparison to the
518 eddy covariance measurements, particularly from mid spring to the end of the summer (Fig.
519 3a and 3e). The peak ET was shifted to late July – early September, while the ET measured
520 from the eddy covariance showed an earlier peak, in March. The large overestimation of the
521 no-DS model was associated with the high ET_0 during the spring and summer ($r=0.91$;
522 $P<0.001$; see also Fig. 2a), which is the driver of the ET model (Eqs. 2, 8 and 12), following
523 the low humidity and augmented radiation load at this time of the year (Rotenberg and Yakir,
524 2011; Tatarinov et al., 2016). However, including the drought stress and the available water
525 factors helped to correct for this overestimation, by linking ET to the available soil water
526 (Fig. 2a), resulting in a good agreement between the model and the eddy covariance estimates
527 (Fig. 3c and 3e; Table 2).

528

529 When comparing the modeled GPP with the EC estimates at Yatir, the model without the
530 drought stress factor (no-DS) produced higher values during both ends of the rainy season
531 (October-November and May-June, Fig. 3b and 3f). In particular, the no-DS model
532 overestimated the GPP during the start of the rainy season (indicated by the arrows in Fig.
533 3b). This was due to the increase in the NDVI following the appearance of ephemeral
534 herbaceous vegetation in the understory of these Mediterranean forests in the beginning of
535 the rainy season, as already pointed out in the previous section (see also Helman et al.,
536 2015b). Also here, the herbaceous vegetation in the understory of Yatir provides a
537 meaningful contribution to the NDVI signal, although it constitutes only a minor component
538 in terms of the biomass and the CO_2 uptake of the forest (Helman et al., 2015b; Rotenberg
539 and Yakir, 2011). Considering the drought stress factor in the RS-Met model thus abridged
540 the RUE, counterbalancing the high contribution of the herbaceous vegetation to the $fPAR$
541 through the NDVI. This also better simulated the drought stress conditions experienced by
542 the woody vegetation, which is the main contributor to the GPP in Yatir, during the dry
543 period (Fig. 3d and 3f).

544

545 These results explicitly show that the drought stress factor is useful in “focusing” the RS data
546 onto the woody vegetation activities (strongly restricted by water shortage at both ends of the
547 rainy season), reducing the impact of other components, such as the peak activities of the



548 understory vegetation that, obviously, does not suffer from water shortage and responds to
549 small early season moisture input (Helman et al., 2014a, n.d.; Mussery et al., 2016).

550

551 5.2. Annual-basis comparisons

552 We then examined the RS-Met model with the drought-stress factor (DS model) on an annual
553 scale, first by comparing the inter-annual variation in the modeled ET with the EC, as well as
554 with the annual rainfall (P) at this site (Fig. 4a). This analysis indicated that the RS-Met
555 model can also reproduce the annual ET with a fair accuracy, showing a moderate but
556 significant correlation with the total annual ET derived from the daily summed EC estimates
557 ($r=0.78$; $P<0.05$; $N=10$; Fig. 4b) and comparable mean annual ET (266 ± 61 vs. 257 ± 58 mm y⁻¹
558 for ET_{MOD} and ET_{EC}, respectively). Both the RS-Met and the EC were significantly
559 correlated with P ($r=0.60$ and 0.93 ; $P=0.05$ and <0.001 , respectively), showing similar
560 patterns in water use (ET/P ratio), though differing in magnitude in some of the years studied
561 (Fig. 4a). In general, the interannual trend in ET/P was much noisier when using ET from the
562 RS-Met compared to that from the EC. This was particularly noted in years when the ET
563 from the RS-Met was significantly different from the EC annual estimates (e.g., 2004, 2006
564 and 2010; Fig. 4a). These differences in annual ET most likely resulted from discrepancies
565 between the two methods in daily estimates during the summer ($r = 0.05$; $P>0.1$ for June-
566 August; Fig. 4c). This is supported by the observation of a 5-fold higher bias between EC and
567 RS-Met summer daily estimates in the years 2004, 2006 and 2010 (bias = -0.146 mm d⁻¹)
568 compared to that from remaining years (bias = -0.029 mm d⁻¹). Additionally, the negative
569 biases imply an average overestimation by the RS-Met model during the summer compared
570 to EC estimates. In contrast, the correlation between the RS-Met and EC was high and
571 significant for daily estimates during the rainy season ($r = 0.80$; $P<0.0001$ for October-May;
572 Fig. 4d). The relatively large discrepancies between RS-Met and EC during the summer
573 indicate the limitation of the RS-Met in estimating relatively low ET values (i.e., <1.0 mm d⁻¹)
574 ¹). This suggests that the water availability factor (f_{wA}) should be adjusted to positive values
575 for a longer period (i.e., longer than the current 2 months applied here following Maselli et al.
576 2014) at the end of the rainy season-beginning of the summer.

577

578 The annual ET, as estimated from both the RS-Met and EC, was higher than the total rainfall
579 amount in some of the years studied (Fig. 4a). A similar pattern was previously reported in
580 forests in water-limited regions (Helman et al., 2016; Raz-Yaseef et al., 2012; Williams et al.,



581 2012). ET higher than rainwater supply indicates that trees use water stored in deep soil
582 layers during wet years in the subsequent dry years (e.g., 2006 and 2008; Raz-Yaseef *et al.*,
583 2012; Barbeta *et al.*, 2015). Thus, the ‘transfer’ of surplus rainwater from previous years
584 should be also taken into consideration when adjusting the model with available water
585 through the f_{DS} and f_{WA} , which are currently calculated only with the seasonal rainfall.

586

587 The modeled GPP (i.e., WS model) was also comparable to the GPP from the EC (765 ± 112
588 vs. 748 ± 124 g C m⁻² y⁻¹, for GPP_{MOD} and GPP_{EC}, respectively), and highly correlated at the
589 annual scale (Fig. 5), with an $r = 0.91$ ($P < 0.001$; $N = 9$) and a low MAE of 52 g C m⁻² y⁻¹
590 (Relative error of *c.* 7%).

591

592

593 6. Testing the models across a rainfall gradient

594 6.1. Comparison with daily ET and GPP from EC

595 We next compared the ET and GPP estimates from the RS-Met model with the field
596 campaign data across the remaining six ecosystems. Comparison between estimates based on
597 the RS-Met model, with (DS) and without (no-DS) the drought stress factor, with those from
598 the EC, indicated significantly higher correlations of the DS models with EC ($P = 0.06$ and
599 $P < 0.01$ for ET and GPP, respectively; Table 2). Only the shrubland site of Kadita showed a
600 higher correlation of the no-DS model with the eddy covariance measurements of the ET.

601 This was due to the continuous ET fluxes throughout the summer period in this relatively
602 moist site, which was not captured by the model. This likely indicates the sensitivity of the
603 current drought stress factor to local conditions and the need to further develop the f_{DS} and
604 improve its application during the dry season, as already pointed out in the previous Section.

605 In general, while using the drought stress factor did not improve (for the ET, $P > 0.1$, as
606 indicated by a two-tailed Student’s *t*-test) or only marginally improved (for the GPP, $P = 0.09$,
607 as indicated by a two-tailed Student’s *t*-test) RS-Met estimates in the non-forest sites, it
608 significantly improved the ET and GPP estimates in forest sites ($P = 0.05$ and $P = 0.016$ for ET
609 and GPP, respectively, as indicated by a two-tailed Student’s *t*-test).

610

611 The RS-Met estimates that included the drought stress factor successfully tracked the
612 seasonality of the measured ET and CO₂ fluxes in all sites, though it should be mentioned
613 that the sites of Kadita and Wady Attir had limited measurements to test this (Fig. 6). Overall,



614 the RS-Met was in good agreement with the eddy covariance measurements, with the cross-
615 site regressions producing highly significant linear fits (Fig. 7a, b; $r=0.82$ and $r=0.86$; and
616 $MAE = 0.47 \text{ mm d}^{-1}$ and $MAE = 1.89 \text{ g C m}^{-2} \text{ d}^{-1}$ for ET and GPP, respectively). The water-
617 use efficiency (WUE; the slope of the regression between ET and GPP in Fig. 7c) was
618 slightly higher at $2.32 \text{ g C kg}^{-1} \text{ H}_2\text{O}$ from the RS-Met compared to the low $1.76 \text{ g C kg}^{-1} \text{ H}_2\text{O}$
619 from EC, but it was within the range reported for similar ecosystems in this region (Tang et
620 al., 2014).

621

622 *6.2. Annual-basis comparisons with ET from PaVI-E*

623 To expand our analysis across the rainfall gradient, and because we do not have continuous
624 estimations from the EC at the six sites, we compared the annual ET from RS-Met with that
625 retrieved from the empirical Pa-VI-E model (Helman et al. 2015) in these sites.

626

627 The results of our comparison showed that the RS-Met and PaVI-E models produced
628 comparable estimates in most of the sites (Fig. 8), with the only exception being the dryland
629 non-forest site of Wady Attir, which showed higher estimates from RS-Met than from PaVI-
630 E ($P<0.01$, as indicated by a Student's *t*-test). In the forest sites, annual ET retrieved from
631 RS-Met was generally higher than that derived from PaVI-E, especially in the wetter site of
632 HaSolelim. Nevertheless, the cross-site regression produced a highly significant linear fit
633 ($r=0.94$; $P<0.01$), confirming the potential use of the RS-Met in assessing ET at the annual
634 scale across the rainfall gradient in those forest and non-forest sites.

635

636 *6.3. Changes in water use efficiency following afforestation across rainfall gradient*

637 We finally used the RS-Met models to assess the impact of afforestation on the water and
638 carbon budgets across the rainfall gradient in Israel by comparing fluxes in the three pine
639 forests (i.e., Yatir, Eshtaol and Birya) with those from the adjacent shrubland sites (i.e., Wady
640 Attir, Modiin and Kadita, respectively). Results showed that the ET significantly increased
641 due to the afforestation of these areas, particularly at the more humid site of Birya (c. 53%),
642 but to a lesser extent at the less humid site of Eshtaol (by c. 20%) and with almost no change
643 in ET in the dryland site of Yatir (4%). The GPP also significantly increased in those three
644 paired-sites. Overall, afforestation across the rainfall gradient was responsible for a
645 significant increase in the WUE in this region (Fig. 9). Nevertheless, the positive change in
646 the WUE decreased when moving from the dry Yatir-Wady Attir paired site (279 mm y^{-1}) to



647 the more humid paired-site of Biryá-Kadita (766 mm y⁻¹; Fig. 9), strengthening the
648 importance of afforestation in dryland areas.

649

650

651 **7. Summary and conclusions**

652 We have tested here biophysical-based models using satellite-derived vegetation index and
653 meteorological data (RS-Met) with and without the inclusion of a seasonal drought stress
654 factor for daily estimations of ET and CO₂ fluxes, validating the models against direct flux
655 measurements from extensive field campaigns at seven evergreen forest and adjacent non-
656 forested ecosystem sites along a steep rainfall gradient in the high-energy water-limited
657 Eastern Mediterranean region. Adding the drought stress factor in the RS-Met models
658 generally improved the performance compared with models without the use of the drought
659 stress factor, particularly in forest sites. Our results show the potential use of simple
660 biophysical remote-sensing-based models to assess ET and GPP on a daily basis and at a
661 moderate spatial resolution of 250 m, even in high-energy water-limited environments. The
662 addition of a drought stress factor to the RS-Met models (based on daily rainfall and radiation
663 and/or temperature data alone) significantly improved the estimation of fluxes in shrublands
664 and especially in forests in this region. Nevertheless, careful attention should be paid to
665 adjusting the drought stress factor to local conditions, with further development of the water
666 availability factor required to improve its application at the end of the rainy season-beginning
667 of the dry period. Using the RS-Met models, we were able to estimate changes in water use
668 efficiency due to afforestation across the rainfall gradient in Israel. Overall, afforestation
669 across our study area was responsible for a significant increase in the WUE. However, the
670 positive change in the WUE decreased when moving from dry (279 mm y⁻¹) to more humid
671 (766 mm y⁻¹) regions, strengthening the importance of afforestation in dryland areas.

672 Finally, the use of the simple RS-Met approach linked to flexible campaign-based ground
673 validation, as demonstrated in this study, represents a powerful basis for the reliable
674 extension of ET and GPP estimates across spatial and temporal scales.

675

676

677 **Acknowledgments**



678 David Helman acknowledges personal grants provided by the Bar-Ilan University
679 Presidential Office (Milgat Hanasi), the JNF-Rieger Foundation, USA, and the Hydrological
680 Service of Israel, Water Authority. S. Rohatyn acknowledges scholarships provided by
681 Ronnie Appleby fund, the Advanced School of Environmental Science of the Hebrew
682 University, and the Israel Ministry of Agriculture. We thank E. Ramati for helping with field
683 work and data processing, G. Fratini for helping with EddyPro, and H. Sagi and A. Perner for
684 technical assistance. We are also grateful to the Meteorological Service of Israel for
685 providing meteorological data and to NASA for making public the MODIS NDVI datasets.
686 This research was partly supported by the Hydrological Service of Israel, Water Authority
687 (Grant No. 4500962964). Flux measurements were made possible through the financial
688 support from the Israel Science Foundation (ISF), Minerva foundation, JNF-KKL, the
689 Hydrological Service of Israel, Water Authority, and C. Wills and R. Lewis program in
690 Environmental Science.

691

692

693 **References**

- 694 Afik, T., 2009. Quantitative estimation of CO₂ fluxes in a semi-arid forest and their
695 dependence on climatic factors. Thesis submitted to R.H. Smith Faculty of Agriculture,
696 Food and Environment of Hebrew University, Rehovot, Israel (in Hebrew). Thesis
697 submitted to R.H. Smith Faculty of Agriculture, Food and Environment of Hebrew
698 University, Rehovot, Israel (in Hebrew).
- 699 Ahlström, A., Raupach, M.R., Schurgers, G., Smith, B., Arneth, A., Jung, M., Reichstein, M.,
700 Canadell, J.G., Friedlingstein, P., Jain, A.K., Kato, E., Poulter, B., Sitch, S., Stocker,
701 B.D., Viovy, N., Wang, Y.P., Wiltshire, A., Zaehle, S., Zeng, N., 2015. The dominant
702 role of semi-arid ecosystems in the trend and variability of the land CO₂ sink. *Science*
703 (80-). 348, 895–899. doi:10.1126/science.aaa1668
- 704 Allen, R.G., Pereira, L.S., Raes, D., 1998. Crop evapotranspiration : guidelines for computing
705 crop water requirements, FAO irrigation and drainage papers;56. FAO, Rome.
- 706 Asaf, D., Rotenberg, E., Tatarinov, F., Dicken, U., Montzka, S.A., Yakir, D., 2013.
707 Ecosystem photosynthesis inferred from measurements of carbonyl sulphide flux. *Nat.*
708 *Geosci* 6, 186–190.
- 709 Aubinet, M., Grelle, A., Ibrom, A., Rannik, S., Moncrieff, J., Foken, T., Kowalski, A.S.,



- 710 Martin, P.H., Berbigier, P., Bernhofer, C., Clement, R., Elbers, J.A., Granier, A.,
711 Grünwald, T., Morgenstern, K., Pilegaard, K., Rebmann, C., Snijders, W., Valentini, R.,
712 Vesa, T., 2000. Estimates of the annual net carbon and water exchange of forests: the
713 EUROFLUX methodology. *Adv. Ecol. Res.* 30, 113–175.
- 714 Baldocchi, D.D., 2003. Assessing the eddy covariance technique for evaluating carbon
715 dioxide exchange rates of ecosystems: past, present and future. *Glob. Chang. Biol.* 9,
716 479–492.
- 717 Barbeta, A., Mejía-Chang, M., Ogaya, R., Voltas, J., Dawson, T.E., Peñuelas, J., 2015. The
718 combined effects of a long-term experimental drought and an extreme drought on the
719 use of plant-water sources in a Mediterranean forest. *Glob. Chang. Biol.* 21, 1213–1225.
720 doi:10.1111/gcb.12785
- 721 Ciais, P., Reichstein, M., Viovy, N., Granier, a, Ogée, J., Allard, V., Aubinet, M.,
722 Buchmann, N., Bernhofer, C., Carrara, a, Chevallier, F., De Noblet, N., Friend, a D.,
723 Friedlingstein, P., Grünwald, T., Heinesch, B., Keronen, P., Knohl, a, Krinner, G.,
724 Loustau, D., Manca, G., Matteucci, G., Miglietta, F., Ourcival, J.M., Papale, D.,
725 Pilegaard, K., Rambal, S., Seufert, G., Soussana, J.F., Sanz, M.J., Schulze, E.D., Vesala,
726 T., Valentini, R., 2005. Europe-wide reduction in primary productivity caused by the
727 heat and drought in 2003. *Nature* 437, 529–533. doi:10.1038/nature03972
- 728 Cleveland, W.S., 1979. Robust locally weighted regression and smoothing scatterplots. *J.*
729 *Am. Stat. Assoc.* 74, 829–836.
- 730 Gamon, J.A., Field, C.B., Goulden, M.L., Griffin, K.L., Hartley, A.E., Joel, G., Peñuelas, J.,
731 Valentini, R., 1995. Relationships between NDVI, canopy structure, and photosynthesis
732 in three Californian vegetation types. *Ecol. Appl.* 28–41.
- 733 Garbulsky, M.F., Filella, I., Verger, a., Peñuelas, J., 2014. Photosynthetic light use efficiency
734 from satellite sensors: From global to Mediterranean vegetation. *Environ. Exp. Bot.* 103,
735 3–11. doi:10.1016/j.envexpbot.2013.10.009
- 736 Garbulsky, M.F., Penuelas, J., Papale, D., Filella, I., 2008. Remote estimation of carbon
737 dioxide uptake by a Mediterranean forest. *Glob. Chang. Biol.* 14, 2860–2867.
738 doi:10.1111/j.1365-2486.2008.01684.x
- 739 Glenn, E., Nagler, P., Huete, A., 2010. Vegetation Index Methods for Estimating



- 740 Evapotranspiration by Remote Sensing. *Surv. Geophys.* 31, 531–555.
741 doi:10.1007/s10712-010-9102-2
- 742 Glenn, E.P., Huete, A.R., Nagler, P.L., Nelson, S.G., 2008. Relationship Between Remotely-
743 sensed Vegetation Indices, Canopy Attributes and Plant Physiological Processes: What
744 Vegetation Indices Can and Cannot Tell Us About the Landscape. *Sensors* 8, 2136–
745 2160. doi:10.3390/s8042136
- 746 Glenn, E.P., Neale, C.M.U., Hunsaker, D.J., Nagler, P.L., 2011. Vegetation index-based crop
747 coefficients to estimate evapotranspiration by remote sensing in agricultural and natural
748 ecosystems. *Hydrol. Process.* 25, 4050–4062. doi:10.1002/hyp.8392
- 749 Helman, D., (under review). Land Surface Phenology: What do we really 'see' from space?
- 750 Helman, D., Givati, A., Lensky, I.M., 2015a. Annual evapotranspiration retrieved from
751 satellite vegetation indices for the eastern Mediterranean at 250 m spatial resolution.
752 *Atmos. Chem. Phys.* 15, 12567–12579. doi:doi:10.5194/acp-15-12567-2015
- 753 Helman, D., Lensky, I.M., Mussery, A., Leu, S., 2014a. Rehabilitating degraded drylands by
754 creating woodland islets: ASSESSING long-term effects on aboveground productivity
755 and soil fertility. *Agric. For. Meteorol.* doi:10.1016/j.agrformet.2014.05.003
- 756 Helman, D., Lensky, I.M., Tessler, N., Osem, Y., 2015b. A phenology-based method for
757 monitoring woody and herbaceous vegetation in Mediterranean forests from NDVI time
758 series. *Remote Sens.* 7, 12314–12335. doi:10.3390/rs70912314
- 759 Helman, D., Lensky, I.M., Yakir, D., Osem, Y., 2016. Forests growing under dry conditions
760 have higher hydrological resilience to drought than do more humid forests. *Glob. Chang.*
761 *Biol.* doi:10.1111/gcb.13551
- 762 Helman, D., Leu, S., Mussery, A., (under review) Leaf-related traits rather than canopy
763 structure determine tree-grass relations in semi-arid environment : interplay of water and
764 light availability 1–17.
- 765 Helman, D., Mussery, A., Lensky, I.M., Leu, S., 2014b. Detecting changes in biomass
766 productivity in a different land management regimes in drylands using satellite-derived
767 vegetation index. *Soil Use Manag.* 30, 32–39. doi:10.1111/sum.12099
- 768 Helman, D., Osem, Y., Yakir, D., Lensky, I.M., 2017. Relationships between climate,
769 topography, water use and productivity in two key Mediterranean forest types with



- 770 different water-use strategies. *Agric. For. Meteorol.* 232, 319–330.
771 doi:<http://dx.doi.org/10.1016/j.agrformet.2016.08.018>
- 772 Huete, A., Didan, K., Miura, T., Rodriguez, E.P., Gao, X., Ferreira, L.G., 2002. Overview of
773 the radiometric and biophysical performance of the MODIS vegetation indices. *Remote*
774 *Sens. Environ.* 83, 195–213.
- 775 Jensen, M.E., Haise, H.R., 1963. Estimating evapotranspiration from solar radiation. *Proc.*
776 *Am. Soc. Civ. Eng. J. Irrig. Drain. Div.* 89, 15–41.
- 777 Jung, M., Reichstein, M., Ciais, P., Seneviratne, S.I., Sheffield, J., Goulden, M.L., Bonan, G.,
778 Cescatti, A., Chen, J., de Jeu, R., Dolman, A.J., Eugster, W., Gerten, D., Gianelle, D.,
779 Gobron, N., Heinke, J., Kimball, J., Law, B.E., Montagnani, L., Mu, Q., Mueller, B.,
780 Oleson, K., Papale, D., Richardson, A.D., Rouspard, O., Running, S., Tomelleri, E.,
781 Viovy, N., Weber, U., Williams, C., Wood, E., Zaehle, S., Zhang, K., 2010. Recent
782 decline in the global land evapotranspiration trend due to limited moisture supply.
783 *Nature* 467, 951–954. doi:10.1038/nature09396
- 784 Kalma, J., McVicar, T., McCabe, M., 2008. Estimating Land Surface Evaporation: A Review
785 of Methods Using Remotely Sensed Surface Temperature Data. *Surv. Geophys.* 29,
786 421–469. doi:10.1007/s10712-008-9037-z
- 787 Klein, T., Rotenberg, E., Tatarinov, F., Yakir, D., 2016. Association between sap flow-
788 derived and eddy covariance-derived measurements of forest canopy CO₂ uptake. *New*
789 *Phytol.* 209, 436–446. doi:10.1111/nph.13597
- 790 Klein, T., Shpringer, I., Fikler, B., Elbaz, G., Cohen, S., Yakir, D., 2013. Relationships
791 between stomatal regulation, water-use, and water-use efficiency of two coexisting key
792 Mediterranean tree species. *For. Ecol. Manage.* 302, 34–42.
- 793 Kool, D., Agam, N., Lazarovitch, N., Heitman, J.L., Sauer, T.J., Ben-Gal, a., 2014. A review
794 of approaches for evapotranspiration partitioning. *Agric. For. Meteorol.* 184, 56–70.
795 doi:10.1016/j.agrformet.2013.09.003
- 796 Llusia, J., Roahtyn, S., Yakir, D., Rotenberg, E., Seco, R., Guenther, A., Peñuelas, J., 2016.
797 Photosynthesis, stomatal conductance and terpene emission response to water
798 availability in dry and mesic Mediterranean forests. *Trees* 30, 749–759.
799 doi:10.1007/s00468-015-1317-x



- 800 Ma, X., Huete, A., Yu, Q., Restrepo-Coupe, N., Beringer, J., Hutley, L.B., Kanniah, K.D.,
801 Cleverly, J., Eamus, D., 2014. Parameterization of an ecosystem light-use-efficiency
802 model for predicting savanna GPP using MODIS EVI. *Remote Sens. Environ.* 154, 253–
803 271. doi:10.1016/j.rse.2014.08.025
- 804 Maselli, F., Barbati, A., Chiesi, M., Chirici, G., Corona, P., 2006. Use of remotely sensed and
805 ancillary data for estimating forest gross primary productivity in Italy. *Remote Sens.*
806 *Environ.* 100, 563–575. doi:10.1016/j.rse.2005.11.010
- 807 Maselli, F., Papale, D., Chiesi, M., Matteucci, G., Angeli, L., Raschi, A., Seufert, G., 2014.
808 Operational monitoring of daily evapotranspiration by the combination of MODIS
809 NDVI and ground meteorological data: Application and evaluation in Central Italy.
810 *Remote Sens. Environ.* 152, 279–290. doi:10.1016/j.rse.2014.06.021
- 811 Maselli, F., Papale, D., Puletti, N., Chirici, G., Corona, P., 2009. Combining remote sensing
812 and ancillary data to monitor the gross productivity of water-limited forest ecosystems.
813 *Remote Sens. Environ.* 113, 657–667. doi:10.1016/j.rse.2008.11.008
- 814 Maseyk, K., Hemming, D., Angert, A., Leavitt, S.W., Yakir, D., 2011. Increase in water-use
815 efficiency and underlying processes in pine forests across a precipitation gradient in the
816 dry Mediterranean region over the past 30 years. *Oecologia* 167, 573–585.
817 doi:10.1007/s00442-011-2010-4
- 818 Maseyk, K.S., Lin, T., Rotenberg, E., Grünzweig, J.M., Schwartz, A., Yakir, D., 2008.
819 Physiology-phenology interactions in a productive semi-arid pine forest. *New Phytol.*
820 178, 603–616.
- 821 Monteith, J.L., 1977. Climate and the efficiency of crop production in Britain. *Phil. Trans. R.*
822 *Soc. Lond. B* 281, 277–294.
- 823 Mussery, A., Helman, D., Leu, S., Budovsky, A., 2016. Modeling herbaceous productivity
824 considering tree-grass interactions in drylands savannah: The case study of Yatir farm in
825 the Negev drylands. *J. Arid Environ.* 124, 160–164. doi:10.1016/j.jaridenv.2015.08.013
- 826 Myneni, R.B., Williams, D.L., 1994. On the relationship between FAPAR and NDVI.
827 *Remote Sens. Environ.* 49, 200–211. doi:10.1016/0034-4257(94)90016-7
- 828 Nagaraja Rao, C.R., 1984. Photosynthetically active components of global solar radiation:
829 Measurements and model computations. *Arch. Meteorol. Geophys. Bioclimatol. Ser. B*



- 830 34, 353–364. doi:10.1007/BF02269448
- 831 Osem, Y., Zangy, E., Bney-Moshe, E., Moshe, Y., 2012. Understory woody vegetation in
832 manmade Mediterranean pine forests: variation in community structure along a rainfall
833 gradient. *Eur. J. For. Res.* 131, 693–704. doi:10.1007/s10342-011-0542-0
- 834 Peñuelas, J., Garbulsky, M.F., Filella, I., 2011. Photochemical reflectance index (PRI) and
835 remote sensing of plant CO₂ uptake. *New Phytol.* 191, 596–9. doi:10.1111/j.1469-
836 8137.2011.03791.x
- 837 Raz-Yaseef, N., Yakir, D., Schiller, G., Cohen, S., 2012. Dynamics of evapotranspiration
838 partitioning in a semi-arid forest as affected by temporal rainfall patterns. *Agric. For.*
839 *Meteorol.* 157, 77–85. doi:10.1016/j.agrformet.2012.01.015
- 840 Reichstein, M., Bahn, M., Ciais, P., Frank, D., Mahecha, M.D., Seneviratne, S.I.,
841 Zscheischler, J., Beer, C., Buchmann, N., Frank, D.C., Papale, D., Rammig, A., Smith,
842 P., Thonicke, K., Velde, M. van der, Vicca, S., Walz, A., Wattenbach, M., 2013.
843 Climate extremes and the carbon cycle. *Nature* 500, 287–295. doi:10.1038/nature12350
- 844 Reichstein, M., Falge, E., Baldocchi, D., Papale, D., Aubinet, M., Berbigier, P., Bernhofer,
845 C., Buchmann, N., Gilmanov, T., Granier, A., Grünwald, T., Havránková, K.,
846 Ilvesniemi, H., Janous, D., Knohl, A., Laurila, T., Lohila, A., Loustau, D., Matteucci,
847 G., Meyers, T., Miglietta, F., Ourcival, J.-M., Pumpanen, J., Rambal, S., Rotenberg, E.,
848 Sanz, M., Tenhunen, J., Seufert, G., Vaccari, F., Vesala, T., Yakir, D., Valentini, R.,
849 2005. On the separation of net ecosystem exchange into assimilation and ecosystem
850 respiration: review and improved algorithm. *Glob. Chang. Biol.* 11, 1424–1439.
851 doi:10.1111/j.1365-2486.2005.001002.x
- 852 Rotenberg, E., Yakir, D., 2011. Distinct patterns of changes in surface energy budget
853 associated with forestation in the semiarid region. *Glob. Chang. Biol.* 17, 1536–1548.
854 doi:10.1111/j.1365-2486.2010.02320.x
- 855 Running, S.W., Nemani, R.R., 1988. Relating seasonal patterns of the AVHRR vegetation
856 index to simulated photosynthesis and transpiration of forests in different climates.
857 *Remote Sens. Environ.* 24, 347–367. doi:10.1016/0034-4257(88)90034-X
- 858 Running, S.W., Nemani, R.R., Heinsch, F.A., Zhao, M., Reeves, M., Hashimoto, H., 2004. A
859 Continuous Satellite-Derived Measure of Global Terrestrial Primary Production.



- 860 Bioscience 54, 547–560. doi:10.1641/0006-3568(2004)054[0547:ACSMOG]2.0.CO;2
- 861 Running, S.W., Thornton, P.E., Nemani, R., Glassy, J.M., 2000. Global Terrestrial Gross and
862 Net Primary Productivity from the Earth Observing System, in: Methods in Ecosystem
863 Science. Ed. O E Sala, R B Jackson, H A Mooney, and R W Howarth, pp. 44–57.
- 864 Schimel, D., Pavlick, R., Fisher, J.B., Asner, G.P., Saatchi, S., Townsend, P., Miller, C.,
865 Frankenberg, C., Hibbard, K., Cox, P., 2015. Observing terrestrial ecosystems and the
866 carbon cycle from space. Glob. Chang. Biol. 21, 1762–1776. doi:10.1111/gcb.12822
- 867 Sims, D.A., Rahman, A.F., Cordova, V.D., El-Masri, B.Z., Baldocchi, D.D., Bolstad, P. V.,
868 Flanagan, L.B., Goldstein, A.H., Hollinger, D.Y., Misson, L., Monson, R.K., Oechel,
869 W.C., Schmid, H.P., Wofsy, S.C., Xu, L., 2008. A new model of gross primary
870 productivity for North American ecosystems based solely on the enhanced vegetation
871 index and land surface temperature from MODIS. Remote Sens. Data Assim. Spec.
872 Issue 112, 1633–1646. doi:10.1016/j.rse.2007.08.004
- 873 Sprintsin, M., Cohen, S., Maseyk, K., Rotenberg, E., Grünzweig, J., Karnieli, a., Berliner, P.,
874 Yakir, D., 2011. Long term and seasonal courses of leaf area index in a semi-arid forest
875 plantation. Agric. For. Meteorol. 151, 565–574. doi:10.1016/j.agrformet.2011.01.001
- 876 Tang, X., Li, H., Desai, A.R., Nagy, Z., Luo, J., Kolb, T.E., Olioso, A., Xu, X., Yao, L.,
877 Kutsch, W., Pilegaard, K., Köstner, B., Ammann, C., 2014. How is water-use efficiency
878 of terrestrial ecosystems distributed and changing on Earth? Sci. Rep. 4, 7483.
879 doi:10.1038/srep07483
- 880 Tatarinov, F., Rotenberg, E., Maseyk, K., Ogée, J., Klein, T., Yakir, D., 2016. Resilience to
881 seasonal heat wave episodes in a Mediterranean pine forest. New Phytol. 210, 485–496.
882 doi:10.1111/nph.13791
- 883 Veroustraete, F., Sabbe, H., Eerens, H., 2002. Estimation of carbon mass fluxes over Europe
884 using the C-Fix model and Euroflux data. Remote Sens. Environ. 83, 376–399.
- 885 Wang, H., Zhao, P., Zou, L.L., McCarthy, H.R., Zeng, X.P., Ni, G.Y., Rao, X.Q., 2014. CO₂
886 uptake of a mature Acacia mangium plantation estimated from sap flow measurements
887 and stable carbon isotope discrimination. Biogeosciences 11, 1393–1411.
888 doi:10.5194/bg-11-1393-2014
- 889 Way, D. a., Oren, R., Kroner, Y., 2015. The space-time continuum: the effects of elevated



- 890 CO₂ and temperature on trees and the importance of scaling. *Plant. Cell Environ.* 38,
891 991–1007. doi:10.1111/pce.12527
- 892 Williams, C.A., Reichstein, M., Buchmann, N., Baldocchi, D., Beer, C., Schwalm, C.,
893 Wohlfahrt, G., Hasler, N., Bernhofer, C., Foken, T., Papale, D., Schymanski, S.,
894 Schaefer, K., 2012. Climate and vegetation controls on the surface water balance:
895 Synthesis of evapotranspiration measured across a global network of flux towers. *Water*
896 *Resour. Res.* 48. doi:10.1029/2011WR011586
- 897 Wu, C., Huang, W., Yang, Q., Xie, Q., 2015. Improved estimation of light use efficiency by
898 removal of canopy structural effect from the photochemical reflectance index (PRI).
899 *Agric. Ecosyst. Environ.* 199, 333–338. doi:10.1016/j.agee.2014.10.017
- 900 Zhao, M., Running, S.W., 2010. Drought-Induced Reduction in Global Terrestrial Net
901 Primary Production from 2000 Through 2009. *Science* (80-.). 329, 940–943.
- 902

903 **Tables**

904 Table 1. Site characteristics and locations divided into two groups of forest (top) and non-
 905 forest (bottom) sites. In each group, sites are arranged from the dry to the humid (from top to
 906 bottom).
 907

Site	Location (Lat, N; Lon, E)	PFT	Dominant species	Grazing	Altitude	P	AF
Yatir	31.3451; 35.0519	CF	<i>P. halepensis</i>	sheep	660	279	0.19
Eshtaol	31.7953; 34.9954	CF	<i>P. halepensis</i>	sheep	385	480	0.34
HaSolelim	32.7464; 35.2317	OF	<i>Q. ithaburensis</i>	cattle	180	543	0.42
Biryra	33.0015; 35.4823	CF	<i>P. halepensis</i>	cattle	750	766	0.63
Wady Attir	31.3308; 34.9905	SH	<i>Phagnalon rupestre</i>	sheep	490	279	0.11
Modiin	31.8698; 35.0125	SH	<i>S. spinosum</i>	cattle	245	480	0.32
Kadita	33.0110; 35.4614	SH	<i>S. spinosum</i>	cattle	815	766	0.63

908
 909 PFT is the plant functional type (CF, Coniferous forest; OF, oak forest; SH, shrubland); Grazing indicates the main
 910 grazing regime in the site; altitude is in meters above sea level; P is the mean annual rainfall (mm y^{-1}); and AF is
 911 the aridity factor calculated as the P to the ET_0 ratio (in mm mm^{-1}).



912 Table 2. Statistics of the comparison between the RS-Met models with the addition of the
 913 drought stress factor (DS) and without its addition (no-DS) and the eddy covariance-derived
 914 measurements.
 915

	ET (mm d ⁻¹)					GPP (g C m ⁻¹ d ⁻¹)				
	N	correlation		MAE		N	correlation		MAE	
		no-DS	DS	no-DS	DS		no-DS	DS	no-DS	DS
Yatir	2228	0.05*	0.76	1.9	0.18	2293	0.56	0.77	1.3	0.8
Eshtaol	47	0.16 ^{ns}	0.64	1.3	1.6	54	0.80	0.90	2.3	2.3
HaSolelim	40	0.72	0.79	2.0	0.8	41	0.80	0.88	2.1	2.1
Birya	57	0.72	0.85	1.8	1.8	57	0.64	0.72	4	3
Wady Attir	28	0.80	0.91	0.5	0.7	29	0.90	0.92	0.7	1.0
Modiin	43	0.62	0.64	1.9	1.0	43	0.89	0.90	1.2	1.2
Kadita	28	0.80	0.67	0.8	1.0	28	0.82	0.88	1.8	1.8

916
 917 The mean absolute error (MAE) is in mm d⁻¹ for the ET and in g C m⁻² d⁻¹ for the GPP. All the correlations were
 918 highly statistically significant at $P < 0.001$, except for the ET model without the drought stress factor (no-DS) at the
 919 forest site of Yatir (*) that was significant at $P = 0.02$, and the site of Eshtaol that was not statistically significant
 920 (ns). The number of days used for the correlation in each site and flux is indicated (N=days).

921 **Figure legends**

922

923 Fig. 1. Views of the 7 study sites along the climatic gradient (a-g) and the newly mobile flux
924 measurement system used in this study (h). Sites include three paired of planted pine forests
925 (*Pinus halepensis*) and adjacent non-forest sites (representing the original environment on
926 which the forests were planted): Yatir (a) and Wady Attir (b), Eshtaol (c) and Modiin (d),
927 Birya (e) and Kadita (f). The seventh site, which is the deciduous oak forest of HaSolelim is
928 shown (d). The three paired sites (a-f) represent the geo-climatic transition from xeric to
929 mesic environments in Israel, respectively.

930

931 Fig. 2. Seasonal evolution of the drought stress factor (f_{DS}) and the main drivers of the ET (a)
932 and GPP (b) models in the forest site of Eshtaol. The K_C from Eq. (9) and the RUE (without
933 the addition of the f_{DS}) are shown together with the ET_o , fVC , PAR, $fPAR$ and the ET and
934 GPP fluxes in this site. The periods when the f_{DS} is particularly useful in reducing the fluxes
935 to a more realistic value due to the shortage in available water are indicated with colored
936 vertical bands.

937

938 Fig. 3. The estimated fluxes derived from the eddy covariance measurements (dots) and RS-
939 Met models at the semiarid pine forest of Yatir. Two models were tested: without considering
940 a drought stress factor (no-DS; grey line in a, b) and with a drought stress factor (DS; black
941 line in c, d). The phase shift in the ET (e) and higher GPP at both ends of the rainy season (f)
942 in the no-DS model are shown for selected years 2009/10 and 2003/4, respectively (Inserts in
943 (e) and (f) show the correlations between modeled and observed fluxes).

944

945 Fig. 4. Annual ET (mm y^{-1}) summed from the daily estimates of the RS-Met model with the
946 drought stress factor (DS) and eddy covariance (EC), and annual rainfall amounts (P) in Yatir
947 for 2003-2014 (a). Linear EC vs. modeled ET regressions of the annual (b) and daily
948 estimates during dry summer (June-August; c) and rainy (October-May; d) seasons. The
949 Pearson's r values of the linear fits are 0.78 ($P < 0.05$; $N = 10$) in (b), 0.05 ($P > 0.1$; $N = 876$) in
950 (c) and 0.80 ($P < 0.0001$; $N = 1570$) in (d). The interannual trends in ET/P from the EC and the
951 model are presented in the upper panel of (a). Note that annual sums of ET from EC and the
952 model in 2012 and 2013, respectively, are not displayed due to the scarcity of available data
953 during these years ($> 50\%$ missing data).

954



955 Fig. 5. Annual GPP ($\text{g C m}^{-2} \text{ y}^{-1}$) summed from the daily estimates of the RS-Met model with
956 the drought stress factor (DS) and eddy covariance (EC) daily estimates in Yatir (a). The
957 linear regression of the EC vs. the model annual GPP (b). The Pearson's r of the linear fit in
958 (b) is 0.91 ($P < 0.05$; $N = 10$). The EC annual GPP for 2009 and 2011 were not calculated due
959 to missing data.

960

961 Fig. 6. The RS-Met model adjusted for drought stress conditions (DS) and the eddy
962 covariance ET (a) and GPP (b) at the 6 forest and non-forested sites.

963

964 Fig. 7. Cross-site correlations between eddy covariance (EC) and RS-Met models with the
965 drought stress factor (DS) of ET (a) and GPP (b) estimates across the six sites; and their ET-
966 GPP relationships (i.e., water-use efficiency; c). Linear fits in (a) and (b) are $\text{ET}_{\text{MOD}} = 0.936$
967 $\text{ET}_{\text{EC}} + 0.281$ ($r = 0.82$; $P < 0.0001$; $N = 243$ d) and $\text{GPP}_{\text{MOD}} = 0.990 \text{ GPP}_{\text{EC}} + 0.515$ ($r = 0.86$;
968 $P < 0.0001$; $N = 252$ d). The slopes of the linear fits in (c) are $2.32 \text{ g C kg}^{-1} \text{ H}_2\text{O}$ and 1.76 g C
969 $\text{kg}^{-1} \text{ H}_2\text{O}$ for MOD-DS and EC, with $r = 0.87$ and 0.65 ($P < 0.0001$; $N = 243$ for both),
970 respectively.

971

972 Fig. 8. Comparison between mean annual ET (2001-2015) from RS-Met (MOD-DS) and the
973 PaVI-E model (Helman et al., 2015a). Pearson's r is 0.90 ($P < 0.01$) with slope = 0.974 and
974 intercept = 40.46 for the regression between the two models' estimates. Error bars indicate
975 the standard deviation. Asterisk indicates significantly different estimates at $P < 0.01$, as
976 indicated by a two-tailed Student's t -test.

977

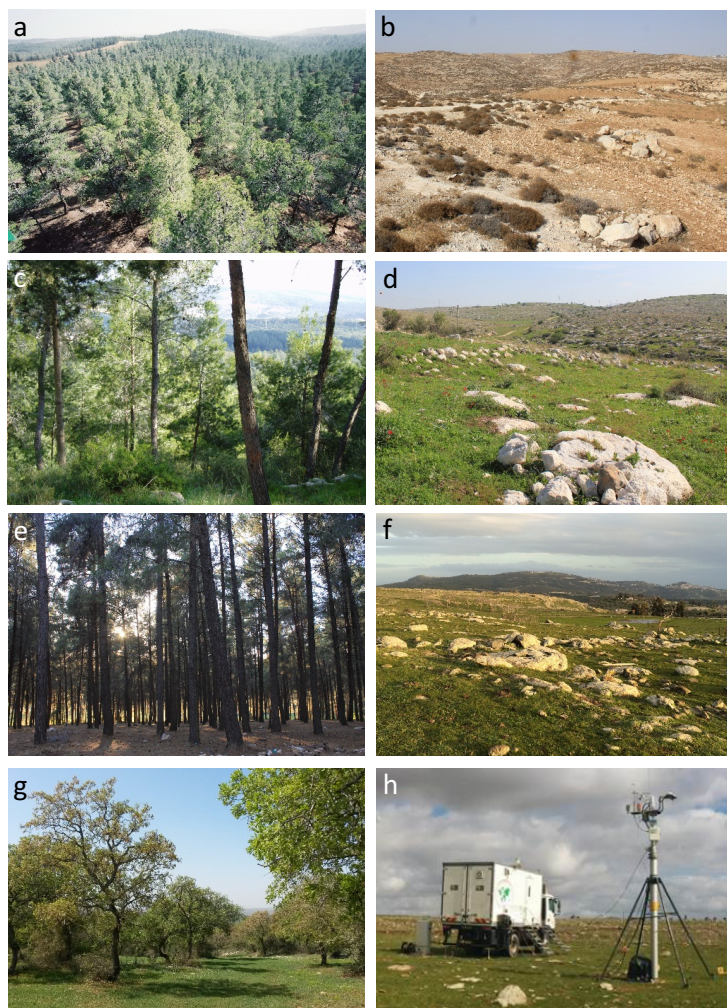
978 Fig. 9. The change in GPP, ET and water use efficiency (WUE; as indicated by the direction
979 of the arrow) attributed to the afforestation (closed symbols) of shrubland areas (open
980 symbols) across a rainfall gradient ($279\text{-}766 \text{ mm y}^{-1}$). The three-paired forest and non-forest
981 sites of Yatir-Wady Attir, Eshtaol-Modiin and Birya-Kadita are indicated with yellow, green
982 and blue colors, respectively. The rainfall level at each paired site is indicated near the arrow
983 (in mm y^{-1}). Note the changing slope of the change in ET and GPP, indicating that the gain in
984 WUE due to afforestation decreases from dry to humid areas.



1 **Figures**

2

3 Figure 1

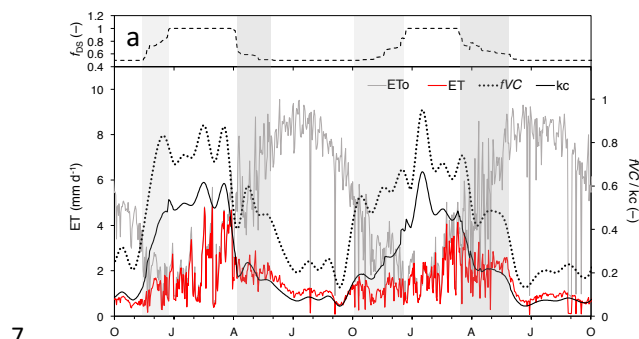


4

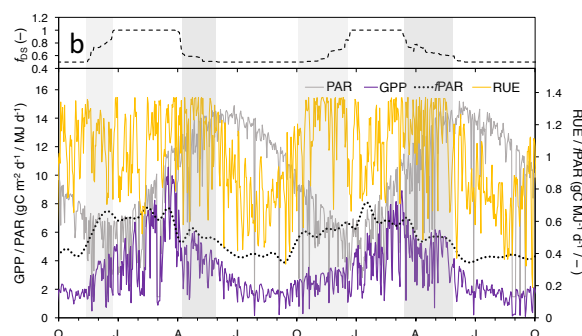


5 Figure 2

6



7



8

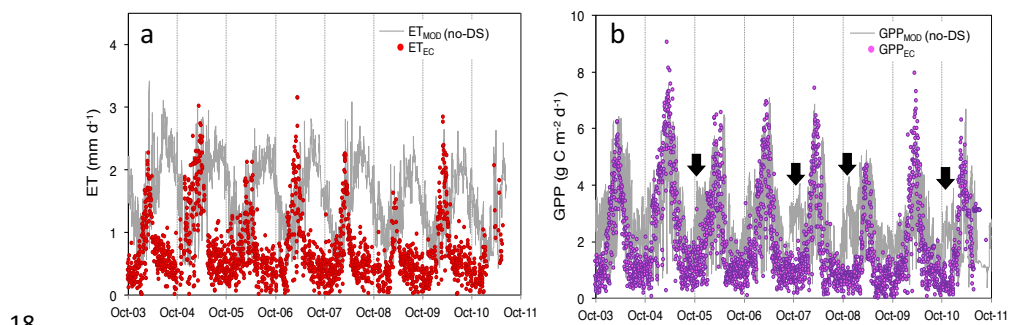
9

10 Fig. 2. Seasonal evolution of the drought stress factor (f_{DS}) and the main drivers of the ET (a)
 11 and GPP (b) models in the forest site of Eshtaol. The K_C from Eq. (9) and the RUE (without
 12 the addition of the f_{DS}) are shown together with the ET_o , fVC , PAR, $fPAR$ and the ET and
 13 GPP fluxes in this site. The periods when the f_{DS} is particularly useful in reducing the fluxes
 14 to a more realistic value due to the shortage in available water are indicated with colored
 15 vertical bands.

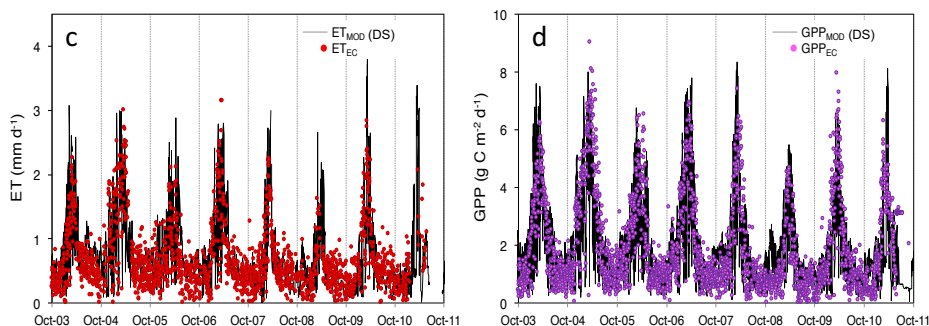


16 Figure 3

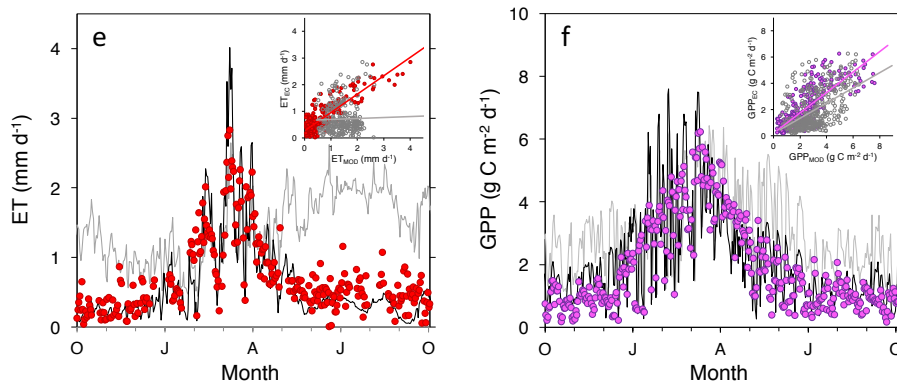
17



19



20



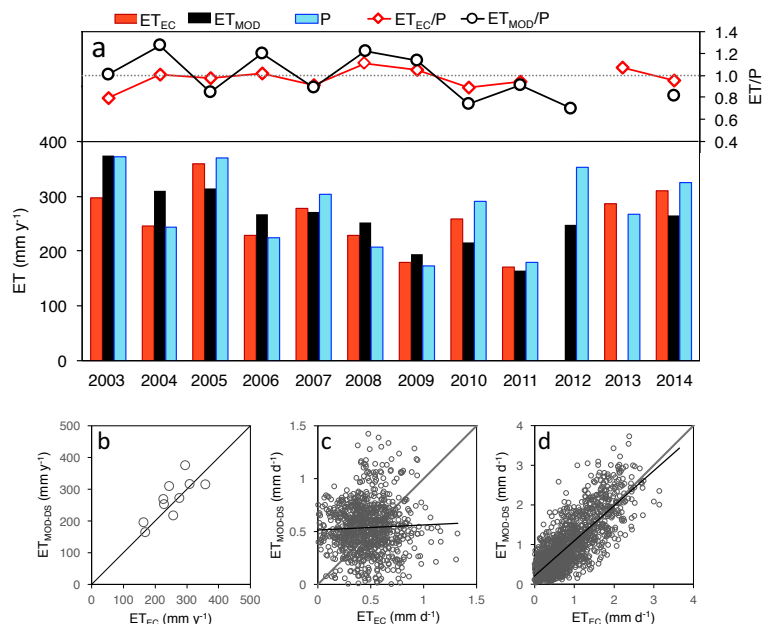
21

22 Fig. 3. The estimated fluxes derived from the eddy covariance measurements (dots) and RS-
 23 Met models at the semiarid pine forest of Yatir. Two models were tested: without considering
 24 a drought stress factor (no-DS; grey line in a, b) and with a drought stress factor (DS; black
 25 line in c, d). The phase shift in the ET (e) and higher GPP at both ends of the rainy season (f)
 26 in the no-DS model are shown for selected years 2009/10 and 2003/4, respectively (Inserts in
 (e) and (f) show the correlations between modeled and observed fluxes).



27 Figure 4

28



29

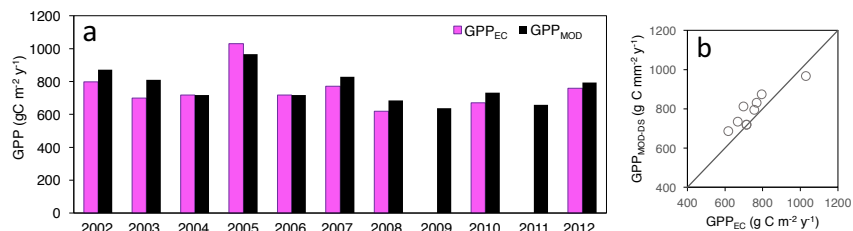
30

31 Fig. 4. Annual ET (mm y⁻¹) summed from the daily estimates of the RS-Met model with the
 32 drought stress factor (DS) and eddy covariance (EC), and annual rainfall amounts (P) in Yatir
 33 for 2003-2014 (a). Linear EC vs. modeled ET regressions of the annual (b) and daily
 34 estimates during dry summer (June-August; c) and rainy (October-May; d) seasons. The
 35 Pearson's r values of the linear fits are 0.78 ($P < 0.05$; $N = 10$) in (b), 0.05 ($P > 0.1$; $N = 876$) in
 36 (c) and 0.80 ($P < 0.0001$; $N = 1570$) in (d). The interannual trends in ET/P from the EC and the
 37 model are presented in the upper panel of (a). Note that annual sums of ET from EC and the
 38 model in 2012 and 2013, respectively, are not displayed due to the scarcity of available data
 39 during these years (>50% missing data).



40 Figure 5

41



42

43

44 Fig. 5. Annual GPP (g C m⁻² y⁻¹) summed from the daily estimates of the RS-Met model with

45 the drought stress factor (DS) and eddy covariance (EC) daily estimates in Yatir (a). The

46 linear regression of the EC vs. the model annual GPP (b). The Pearson's r of the linear fit in

47 (b) is 0.91 ($P < 0.05$; $N = 10$). The EC annual GPP for 2009 and 2011 were not calculated due

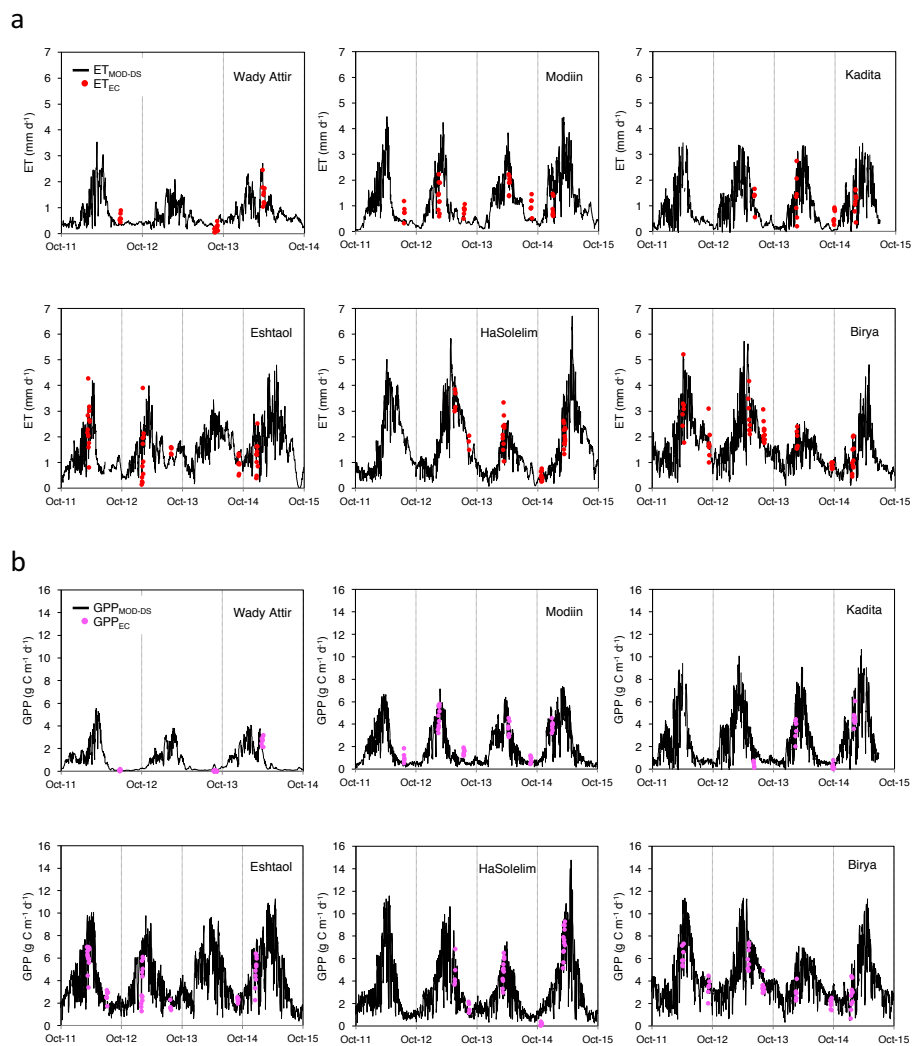
48 to missing data.

49



50 Figure 6

51



52

53

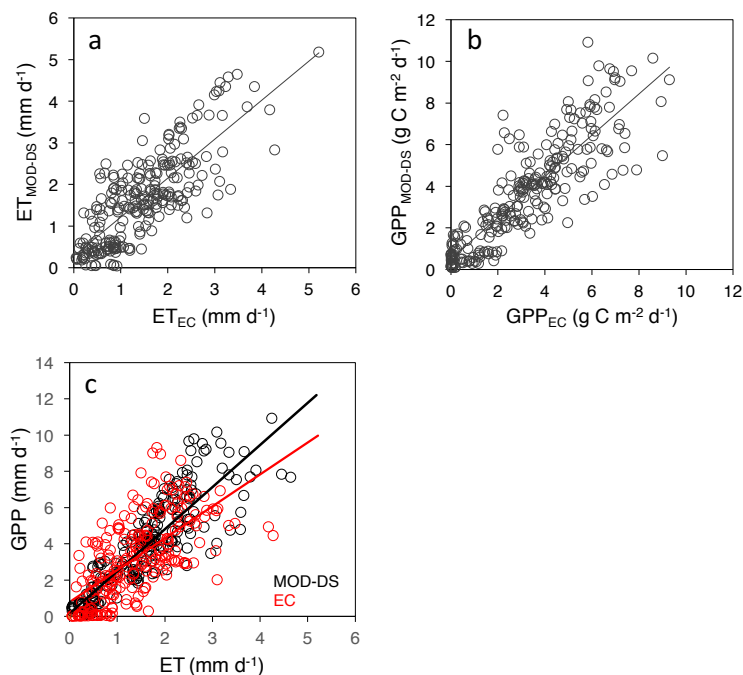
54 Fig. 6. The RS-Met model adjusted for drought stress conditions (DS) and the eddy

55 covariance ET (a) and GPP (b) at the 6 forest and non-forested sites.



56 Figure 7

57



58

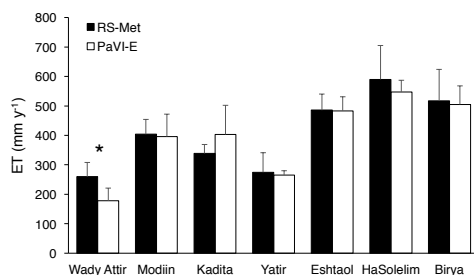
59

60 Fig. 7. Cross-site correlations between eddy covariance (EC) and RS-Met models with the
61 drought stress factor (DS) of ET (a) and GPP (b) estimates across the six sites; and their ET-
62 GPP relationships (i.e., water-use efficiency; c). Linear fits in (a) and (b) are $ET_{MOD} = 0.936$
63 $ET_{EC} + 0.281$ ($r = 0.82$; $P < 0.0001$; $N = 243$ d) and $GPP_{MOD} = 0.990 GPP_{EC} + 0.515$ ($r = 0.86$;
64 $P < 0.0001$; $N = 252$ d). The slopes of the linear fits in (c) are $2.32 \text{ g C kg}^{-1} \text{ H}_2\text{O}$ and 1.76 g C
65 $\text{kg}^{-1} \text{ H}_2\text{O}$ for MOD-DS and EC, with $r = 0.87$ and 0.65 ($P < 0.0001$; $N = 243$ for both),
66 respectively.



67 Figure 8

68



69

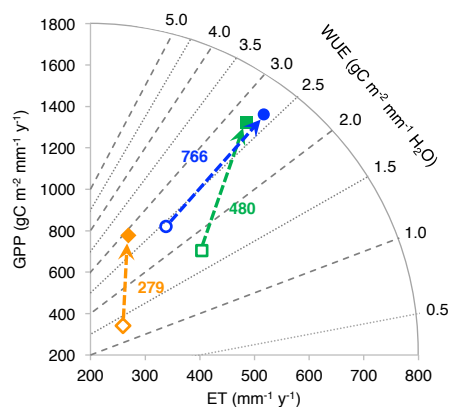
70

71 Fig. 8. Comparison between mean annual ET (2001-2015) from RS-Met (MOD-DS) and the
72 PaVI-E model (Helman *et al.*, 2015a). Pearson's r is 0.90 ($P < 0.01$) with slope = 0.974 and
73 intercept = 40.46 for the regression between the two models' estimates. Error bars indicate
74 the standard deviation. Asterisk indicates significantly different estimates at $P < 0.01$, as
75 indicated by a two-tailed Student's t -test.



76 Figure 9

77



78

79

80 Fig. 9. The change in GPP, ET and water use efficiency (WUE; as indicated by the direction
81 of the arrow) attributed to the afforestation (closed symbols) of shrubland areas (open
82 symbols) across a rainfall gradient (279-766 mm y⁻¹). The three-paired forest and non-forest
83 sites of Yatir-Wady Attir, Eshtaol-Modiin and Birya-Kadita are indicated with yellow, green
84 and blue colors, respectively. The rainfall level at each paired site is indicated near the arrow
85 (in mm y⁻¹). Note the changing slope of the change in ET and GPP, indicating that the gain in
86 WUE due to afforestation decreases from dry to humid areas.